
Categorical Flow Matching on Statistical Manifolds

Chaoran Cheng

University of Illinois Urbana-Champaign
chaoran7@illinois.edu

Jiahan Li

Peking University
lijiahanc@pku.edu.cn

Jian Peng

University of Illinois Urbana-Champaign
jianpeng@illinois.edu

Ge Liu

University of Illinois Urbana-Champaign
geliu@illinois.edu

Abstract

We introduce Statistical Flow Matching (SFM), a novel and mathematically rigorous flow-matching framework on the manifold of parameterized probability measures inspired by the results from information geometry. We demonstrate the effectiveness of our method on the discrete generation problem by instantiating SFM on the manifold of categorical distributions whose geometric properties remain unexplored in previous discrete generative models. Utilizing the Fisher information metric, we equip the manifold with a Riemannian structure whose intrinsic geometries are effectively leveraged by following the shortest paths of geodesics. We develop an efficient training and sampling algorithm that overcomes numerical stability issues with a diffeomorphism between manifolds. Our distinctive geometric perspective of statistical manifolds allows us to apply optimal transport during training and interpret SFM as following the steepest direction of the natural gradient. Unlike previous models that rely on variational bounds for likelihood estimation, SFM enjoys the exact likelihood calculation for arbitrary probability measures. We manifest that SFM can learn more complex patterns on the statistical manifold where existing models often fail due to strong prior assumptions. Comprehensive experiments on real-world generative tasks ranging from image, text to biological domains further demonstrate that SFM achieves higher sampling quality and likelihood than other discrete diffusion or flow-based models.

1 Introduction

Recently, conditional flow matching (CFM) models [36] have achieved remarkable success in various generative domains including image generation [36, 18, 28], molecule [55, 54, 30] and protein design [62, 11], and sequence generation [56, 37, 13]. While attempts to generalize CFM and diffusion models to discrete categorical data have been made, they typically exert ad hoc assumptions on the structure of the discrete distribution. One group of work relies on stochastic jumps of Markov chains in either the discrete-time [6, 37, 1] or continuous-time setting [12, 51, 13] that discards the continuous nature of the underlying categorical distributions. Other work directly works with the probability simplex [7, 56] or the corresponding logit space [27, 38, 23] with potentially imperfect assumptions that fail to capitulate the underlying true geometry of the statistical manifold. Furthermore, likelihood is often approximated by variational bounds in previous discrete generative models due to the lack of tractable exact likelihood.

We propose to incorporate the intrinsic geometry of the *statistical manifold* by viewing categorical data as points on the statistical manifold of categorical distributions. Inspired by the mathematical results from information theory, we utilize the Fisher information metric [48] to naturally equip

such a manifold with a Riemannian structure and develop an efficient generative training scheme for learning the vector fields without stability issues. We summarize our contributions as the following:

(1) We propose *Statistical Flow Matching* (SFM), a novel and mathematically rigorous generative framework on the manifold of parameterized probability measures. SFM does not pose any prior assumptions on the statistical manifold but instead deduces its intrinsic geometry via mathematical tools. To tackle the discrete generation problem, we instantiate SFM on the manifold of categorical distributions. We deduce closed-form exponential and logarithm maps and develop an efficient flow-matching training algorithm that avoids numerical issues by leveraging a diffeomorphism between manifolds. SFM effectively leverages the intrinsic geometric properties by following the shortest paths of geodesics between the noise and target distributions on the statistical manifold.

(2) Our distinctive geometric perspective of the statistical manifold allows us to further apply optimal transport during training and derive tractable exact likelihood for any given sample of probability measure, both of which are unachievable for most existing methods. We also introduce new theoretical insights by establishing connections among Riemannian flow matching, information geometry, and natural gradient descent, which allows us to interpret SFM as following the steepest descent of the *natural gradient* from the optimization angle.

(3) We demonstrated with a toy example on simplex that SFM can learn more complex patterns on the statistical manifold where existing models often fail due to impromptu prior assumptions. We further conducted extensive experiments on diverse real-world discrete generation tasks involving computer vision, natural language processing, and bioinformatics. SFM consistently outperformed existing diffusion or flow-based models and also achieved comparable results with autoregressive models on character-level generation.

2 Preliminary

2.1 Information Geometry

In this work, we are interested in learning a parameterized family of probability measures. It is known from information theory that all probability measures over the sample space form the structure known as *statistical manifold*. Mathematically, consider probability densities $p = \frac{d\mu}{d\nu} : \mathcal{X} \rightarrow \mathbb{R}$ defined by the Radon-Nikodym derivative where μ is a probability measure on the sample space \mathcal{X} and ν is the reference measure on \mathcal{X} . Suppose the statistical manifold $\mathcal{P} = \mathcal{P}(\mathcal{X}) = \{p : \int_{\mathcal{X}} d\mu = \int_{\mathcal{X}} p(x; \theta) d\nu = 1\}$ is parameterized by $\theta = (\theta_1, \theta_2, \dots, \theta_n) \in \Theta$, this parameterization naturally provides a coordinate system for \mathcal{P} on which each point is a probability measure μ with the corresponding probability density function $p(x; \theta)$. The *Fisher information metric* is defined as:

$$g_{jk}(\theta) = \mathbb{E}_X \left[\frac{\partial \log p(X; \theta)}{\partial \theta_j} \frac{\partial \log p(X; \theta)}{\partial \theta_k} \right] = \int_{\mathcal{X}} \frac{\partial \log p(x; \theta)}{\partial \theta_j} \frac{\partial \log p(x; \theta)}{\partial \theta_k} p(x; \theta) d\nu \quad (1)$$

Rao demonstrated in his seminal paper [48] that statistical manifold can be equipped with the Fisher information metric to obtain a Riemannian structure, the study of which is known as *information geometry* [5, 4, 8]. This geometric view of statistical manifolds allows us to derive key geometric concepts for our statistical flow matching framework. For example, a *geodesic* $\gamma(t) : [0, 1] \rightarrow \mathcal{P}$ defines a “shortest” path (under the Riemannian metric) connecting two probability measures on the statistical manifold. The *geodesic distance* between two probability measures, also known as the Fisher-Rao distance [48], measures the similarity between them. The *tangent space* $T_{\mu}(\mathcal{P})$ at a point $\mu \in \mathcal{P}$ can be naturally identified with the affine subspace $T_{\mu}(\mathcal{P}) = \{\nu | \int_{\mathcal{X}} d\nu = 0\}$ where each element ν is a signed measure over \mathcal{X} . The *exponential map* $\exp_{\mu} : T_{\mu}(\mathcal{P}) \rightarrow \mathcal{P}$ and *logarithm map* $\log_{\mu} : \mathcal{P} \rightarrow T_{\mu}(\mathcal{P})$ can also be defined on the statistical manifold. While the geodesic for a parameterized family of probability measures can be obtained numerically by solving the geodesic equation when closed-form expression is unknown (see Appendix A.1), it usually requires expensive simulations. Fortunately, closed-form geodesic distances are available for many common distributions including categorical, multinomial, and normal distributions [42], which motivate our method.

2.2 Conditional Flow Matching on Riemannian Manifold

The conditional flow matching (CFM) framework [36] provides a simple yet powerful approach to generative modeling by learning a time-dependent vector field that pushes the prior noise distribution

to any target data distribution. Such a flow-based model can be viewed as the continuous generalization of the score matching (diffusion) model [52, 53, 25] while allowing for a more flexible design of the denoising process. The Riemannian flow matching framework [15] further extends CFM to general manifolds on which a well-defined distance metric can be efficiently computed.

Consider a smooth Riemannian manifold \mathcal{M} with the Riemannian metric g , a *probability path* $p_t : [0, 1] \rightarrow \mathcal{P}(\mathcal{M})$ is a curve of probability densities over \mathcal{M} . A *flow* $\psi_t : [0, 1] \times \mathcal{M} \rightarrow \mathcal{M}$ is a time-dependent diffeomorphism defined by a time-dependent vector field $u_t : [0, 1] \times \mathcal{M} \rightarrow T\mathcal{M}$ via the ordinary differential equation (ODE): $\frac{d}{dt}\psi_t(x) = u_t(\psi_t(x))$. The flow matching objective directly regresses the vector field u_t with a time-dependent neural net $v(x_t, t)$ where $x_t := \psi_t(x)$. However, this objective is generally intractable. Both [36, 15] demonstrated that a tractable objective can be derived by conditioning on the delta measure δ_{x_1} at $t = 1$ of the probability path. The Riemannian flow matching objective can be formulated as [15]

$$\mathcal{L} = \mathbb{E}_{t \sim U[0,1], x_0 \sim p_0(x), x_1 \sim q(x)} [\|v(x_t, t) - u_t(x_t|x_0, x_1)\|_g^2] \quad (2)$$

where q is the data distribution, p_0 is the prior distribution, and $x_t := \psi_t(x|x_0, x_1)$ denotes the conditional flow. [15] further demonstrated that if the exponential map and logarithm map can be evaluated in closed-form, the condition flow can be defined as $x_t = \exp_{x_0}(t \log_{x_0} x_1)$, and the corresponding vector field can be calculated as $u_t(x_t|x_0, x_1) = \frac{d}{dt}x_t = \log_{x_t}(x_1)/(1-t)$. We also adapt this formulation for our statistical flow, which we will elaborate on in the next section. We note that, since we are working with manifolds of probability measures $\mathcal{M} = \mathcal{P}(\mathcal{X})$, we will use p, q for probability densities *over* the manifold $\mathcal{P}(\mathcal{X})$ and μ, ν for probability measures (or probability masses for discrete distributions) *on* the manifold $\mathcal{P}(\mathcal{X})$ to avoid confusion.

3 Method

Different from previous work that treated each distribution separately, we adopt an integral viewpoint toward the manifold of probability distributions. In this section, we focus on the statistical manifold of categorical distributions to demonstrate the application of our method on discrete generation tasks. However, we emphasize that our proposed SFM is applicable to any statistical manifold with a closed-form geodesic distance and can be broadly used in generative tasks targeting probability measures on the statistical manifold.

3.1 Statistical Manifold of Categorical Distributions

Consider the discrete sample space $\mathcal{X} = \{1, 2, \dots, n\}$, an n -class categorical distribution over \mathcal{X} can be parameterized by n parameters $\mu_1, \mu_2, \dots, \mu_n$ such that $\sum_{i=1}^n \mu_i = 1, \mu_i \geq 0$. In this way, the reference measure ν is the counting measure and the probability measure μ can be written as the convex combination of the canonical basis of delta measures $\{\delta^i\}_{i=1}^n$ over \mathcal{X} : $\mu = \sum_{i=1}^n \mu_i \delta^i$. Geometrically, this manifold can be visualized as the $(n-1)$ -dimensional simplex Δ^{n-1} . The geodesic distance between two categorical distributions is given in [48, 42] as

$$d_{\text{cat}}(\mu, \nu) = 2 \arccos \left(\sum_{i=1}^n \sqrt{\mu_i \nu_i} \right) \quad (3)$$

The target space at a point μ can be identified with $T_\mu(\mathcal{P}) = \{u \mid \sum_{i=1}^n u_i = 0\}$ and the corresponding inner product at point μ is defined as

$$\langle u, v \rangle_\mu = \sum_{i=1}^n \frac{u_i v_i}{\mu_i}, \quad \mu \in \mathcal{P}^\circ, u, v \in T_\mu(\mathcal{P}) \quad (4)$$

where \mathcal{P}° denotes the interior of the statistical manifold \mathcal{P} . Note that the inner product is ill-defined on the boundary, causing numerical issues near the boundary. To circumvent this issue, we introduce the following diffeomorphism:

$$\pi : \mathcal{P} \rightarrow S_+^{n-1}, \quad \mu_i \mapsto x_i = \sqrt{\mu_i} \quad (5)$$

which maps the original statistical manifold to the positive orthant of a unit $(n-1)$ -sphere $S_+^{n-1} = \{x \mid \sum_{i=1}^n x_i^2 = 1, x_i \geq 0\}$ (see Fig.2). Note that we have $\|\pi(\mu)\|_2^2 = \sum_{i=1}^n \sqrt{\mu_i}^2 = \sum_{i=1}^n \mu_i = 1$. The geodesic on S_+^{n-1} follows the great circle, and the following proposition holds between the geodesic distance on S_+^{n-1} and \mathcal{P} :

Proposition 1.

$$d_S(\pi(\mu), \pi(\nu)) = \frac{1}{2} d_{\text{cat}}(\mu, \nu), \quad \mu, \nu \in \mathcal{P} \quad (6)$$

A proof is provided in Appendix A.3). This indicates that we can work with the geodesic distance on the unit sphere instead with up to a constant factor:

$$d_S(x, y) = \arccos(\langle x, y \rangle), \quad x, y \in S_+^{n-1} \quad (7)$$

The geodesic distance d_S and the inner product $\langle \cdot, \cdot \rangle$ are well-defined for the boundary, and we found this transform led to the practical stabilized training of the flow model. Visualizations of the Riemannian geometry on the statistical manifold of 3-class categorical distributions and the corresponding Euclidean geometry on the simplex are provided in Fig.1 for comparison. The straight lines under the Euclidean assumptions fail to capture the true curved geometry of the statistical manifold.

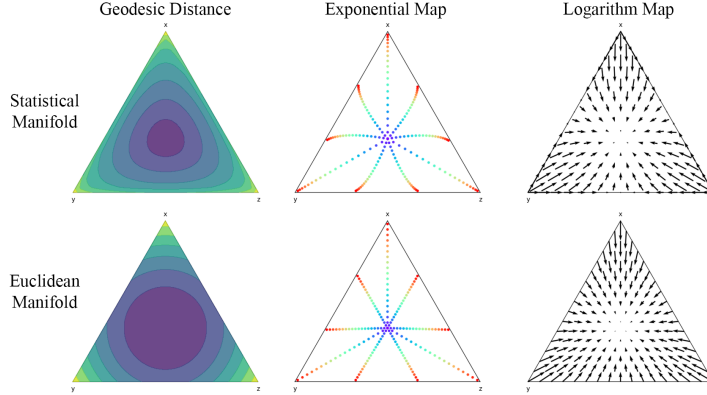


Figure 1: The Riemannian geometry of the statistical manifold for categorical distributions in comparison to Euclidean geometry on the simplex. **Left:** Contours for the geodesic distances to $\mu_0 = (1/3, 1/3, 1/3)$. **Middle:** Exponential maps (geodesics) from μ_0 to different points near the boundary. **Right:** Logarithm maps (vector fields) to μ_0 .

3.2 Statistical Flow Matching

We provide the analytical form of the exponential and logarithm maps on the statistical manifold of categorical distributions in Appendix A.3. Although it is possible to directly learn the vector field following the loss in Eq.2, such a direct parameterization has numerical issues near the boundary. As described in Sec.3.1, we apply the diffeomorphism π in Eq.5 to derive a more stable training objective on the spherical manifold:

$$\mathcal{L}_{\text{SFM}} = \mathbb{E}_{t \sim U[0,1], x_0 \sim \pi(p_0(\mu)), x_1 \sim \pi(q(\mu))} [\|v(x_t, t) - u_t^S(x_t|x_0, x_1)\|_2^2] \quad (8)$$

where p_0 is the prior noise distribution over \mathcal{P} and q is the data distribution. $v : S_+^{n-1} \times [0, 1] \rightarrow TS_+^{n-1}$ is a learnable time-dependent vector field network that maps the interpolant x_t on the unit sphere to a tangent vector in the tangent bundle TS_+^{n-1} . The ground truth conditional vector field u^S is calculated using the exponential and logarithms maps on the sphere (Appendix A.2). The overall training and inference scheme is visualized in Fig.2 and described in Appendix Alg. 2 - 3.

We further implement a Euclidean flow matching model on the probability simplex with linear interpolation between the noises and the target distributions. Though linear flow matching offers “straight” lines under the Euclidean assumption, it is unaware of the intrinsic geometric properties of the statistical manifold and turns out to trace longer paths in terms of the Riemannian metric. The objective for linear flow matching can be described as

$$\mathcal{L}_{\text{LinearFM}} = \mathbb{E}_{t \sim U[0,1], \mu_0 \sim p_0(\mu), \mu_1 \sim q(\mu)} [\|v(\mu_t, t) - (\mu_1 - \mu_0)\|_2^2] \quad (9)$$

In the discussion above, we assume a single data dimension on the statistical manifold. This can be extended to any data dimension by treating them as independent channels of the input. In practice,

each probability measure on the simplex is represented by a matrix $X \in [0, 1]^{D \times n}$ where D is the data dimension and each row sums to 1. The priors are independently sampled from the uniform distribution over the $(n - 1)$ -simplex and each data dimension is independently interpolated with the same timestep $t \sim U[0, 1]$. The flow model, on the other hand, takes all the data dimensions as input to capture the dependence between different dimensions. During sampling, existing ODE solvers and the simple Euler method are used to integrate the vector field through time to obtain the final categorical distributions. Discrete samples are then drawn from the generated categorical distributions for evaluation. Details regarding model parameterization and sampling are further described in Appendix C.1 and C.2.

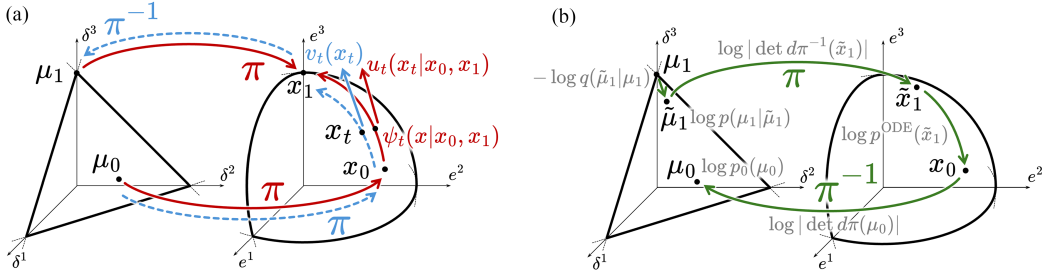


Figure 2: Statistical flow matching (SFM) framework. **(a)** During training (Sec.3.2), probability measures on \mathcal{P} are mapped to S_+^{n-1} via diffeomorphism π to compute the time-dependent vector field (in red). During inference, the learned vector field generates the trajectory on S_+^{n-1} and we map the outcome of ODE back to \mathcal{P} (in blue). **(b)** In the NLL calculation for one-hot examples (Sec.3.5), the probability density is marginalized over a small neighborhood of some delta measure to avoid undefined behaviors at the boundary (in green).

3.3 Optimization View of Statistical Flow Matching

We further provide an interpretation of our proposed statistical flow matching framework from the perspective of an optimization problem. For a generative model on a statistical manifold, we want to minimize the discrepancy between the target distributions and the generated distributions. Naturally, the Kullback-Leibler divergence $D_{\text{KL}}(\mu(\theta) \parallel \mu(\theta_1))$ can be used as a measure of statistical distance. We note that the Fisher information metric can be obtained as the Hessian of the KL divergence with respect to the parameter θ . This can be demonstrated by the fact that the KL divergence reaches the global minimum of 0 at $\theta = \theta_1$, so all first-order partial derivatives are zero and the Hessian is positive semi-definite. Therefore, Taylor expansion of KL divergence at θ_1 gives

$$D_{\text{KL}}(\mu(\theta) \parallel \mu(\theta_1)) \approx \frac{1}{2} \sum_{jk} \Delta\theta_j \Delta\theta_k \left. \frac{\partial^2}{\partial\theta_j \partial\theta_k} D_{\text{KL}}(\mu(\theta) \parallel \mu(\theta_1)) \right|_{\theta=\theta_1} = \frac{1}{2} \sum_{jk} \Delta\theta_j \Delta\theta_k g_{jk}(\theta_1) \quad (10)$$

Therefore, the Fisher information metric defines a second-order optimization scheme for the KL divergence by following the “steepest” direction of the Hessian. In fact, this idea has already been explored by previous work on optimization known as *natural gradient descent* [2, 3] and has been applied to training machine learning models [46, 40, 44]. Instead of optimizing along the normal gradient, the natural gradient is defined as $\tilde{\nabla} \mathcal{L} = F^{-1} \nabla \mathcal{L}$ where F is the Fisher information matrix estimated from a batch of sampled data. Results established in [2, 40] demonstrated that stochastic natural gradient descent is asymptotically “Fisher efficient” and is indeed the steepest descent direction in the manifold of distributions where distance is measured in small local neighborhoods by the KL divergence. Following the geodesic defined by the Fisher information metric, our SFM framework also shares these benefits with an additional advantage of analytical expressions for geodesics, as we focus on the family of categorical distributions instead of general statistical models.

3.4 Optimal Transport on Statistical Manifold

The geometric viewpoint of the statistical manifold offers a continuous and differentiable formulation of generative modeling and also provides a robust way to measure the distance between two categorical

distributions via the well-defined geodesic distance in Eq.(3). In contrast, the Markov chain-based methods cannot establish a robust distance measure due to the stochastic jumps between discrete states. Inspired by the optimal transport formulation in previous work [43, 20, 62], we naturally extend it to our statistical setting in which the cost is defined by averaging the statistical distances over data dimensions as $d_{\text{cat}}(X, Y) = \frac{1}{D} \sum_{k=1}^D d_{\text{cat}}(\mu^{(k)}, \nu^{(k)})$ for $X = \{\mu^{(k)}\}_{k=1}^D, Y = \{\nu^{(k)}\}_{k=1}^D$. An optimal assignment of the initial noises to the target data distributions can potentially lead to more efficient training, which we demonstrated empirically in our ablation studies.

3.5 Exact Likelihood Calculation

Unlike diffusion-based models which rely on variational lower bounds for likelihood estimation, our proposed method shares the continuous normalizing flow’s capability of exact likelihood calculation. For an arbitrary test sample $x \in \mathcal{M}$, using the change of measure formula, the likelihood can be modeled by the continuity equation [15, 41]:

$$\frac{\partial}{\partial t} \log p_t(x_t) + \text{div}_g(v_t)(x_t) = 0 \quad (11)$$

where div_g is the Riemannian divergence and $v_t(x_t) := v(x_t, t)$ is the time-dependent vector field. In this way, the push-forward probability measures $p_t(x_t)$ defined via the learned flow can be obtained as the integral of the Riemannian divergence back through time on the simulated trajectory x_t . Following [10, 7], we define the ODE log-likelihood as:

$$\log p^{\text{ODE}}(x_1) = \int_1^0 \text{div}_g(v_t)(x_t) dt \quad (12)$$

where the trajectory x_t is obtained by solving the differential equation $\frac{\partial}{\partial t} x_t = v_t(x_t)$ reverse through time with the initial condition x_1 at $t = 1$. In this way, we have $\log p(x_1) = \log p^{\text{ODE}} + \log p_0(x_0)$ where $\log p_0(x_0)$ is the log-likelihood of the prior distribution at data point x_0 . In practice, we follow previous work [7] to use Hutchinson’s trace estimator [29] to efficiently obtain an unbiased estimation of the divergence using standard normal random variables. To further account for the transform π from \mathcal{P} to S_+^{n-1} and the reverse transform π^{-1} , additional change of measure formulae need to be applied. Consider the push-forward of the probability measure p over \mathcal{P} under the diffeomorphism π defined by $\pi_* p(V) := p(\pi^{-1}V)$, we have the change of measure identity $\pi_* p(\pi(\mu)) |\det d\pi(\mu)| = p(x)$ for $x = \pi(\mu)$. Therefore, adding the two log-determinant of the push-forward measures, the log-likelihood can be formulated as

$$\log p_1(\mu_1) = \log |\det d\pi^{-1}(x_1)| + \log p^{\text{ODE}}(x_1) + \log |\det d\pi(\mu_0)| + \log p_0(\mu_0) \quad (13)$$

The above formula is well-defined for all interior points of \mathcal{P} , but the change of measure terms are undefined on the boundary. This can be understood as the fact that discrete likelihoods can be arbitrarily high [58]. Following [7], we derive a variational lower bound for the likelihood as the marginalized probability over the small neighborhood of the delta measure $\mu_1 = \delta$ at the boundary:

$$\log p(\delta) \geq \mathbb{E}_{q(\tilde{\mu}_1|\delta)} [-\log q(\tilde{\mu}_1|\delta) + \log p(\delta|\tilde{\mu}_1) + \log p_1(\tilde{\mu}_1)] \quad (14)$$

where $q(\tilde{\mu}_1|\delta)$ can be viewed as the forward noising probability at $\tilde{\mu}_1$ which is close to δ with a closed-form likelihood. $p(\delta|\tilde{\mu}_1)$ is the categorical likelihood (cross-entropy) and $p_1(\tilde{\mu}_1)$ is the model likelihood in Eq.(13). The overall workflow of calculating NLL is demonstrated in Fig.2, and more details regarding likelihood computation can be found in Appendix B.1. It is worth mentioning that the continuous likelihood calculated here is defined with respect to the probability distribution over the statistical manifold \mathcal{P} . In contrast, the bits-per-dimension score for autoregressive models is usually defined with respect to a specific categorical distribution on \mathcal{P} and therefore not comparable, as was also noted in [7].

4 Experiments

Our proposed SFM framework can be leveraged to approximate arbitrary distribution over \mathcal{P} , i.e., any distribution over the parameterized family of probability measures. We first demonstrate this with the toy example of a Swiss roll distribution on the probability simplex. We then conduct

extensive experiments on real-world datasets for discrete generation across various domains including computer vision, natural language processing, and bioinformatics to demonstrate the effectiveness of our proposed model. We train and evaluate two different versions of the SFM framework: **SFM w/ OT** for our proposed model with optimal transport during training and **SFM w/o OT** for the model without optimal transport. We also implement a linear flow matching model on the probability simplex using the loss in Eq.(9) as an additional baseline, for which we dub **LinearFM**. For discrete data, we always use Eq.(14) to obtain finite negative log-likelihood (NLL). More details regarding model architectures and the experimental setup can be found in Appendix C.

4.1 Toy Example: Swiss Roll on Simplex

We project the Swiss roll dataset onto the 2-simplex with some additional margins to make sure no point resides on the boundary. We used a time-dependent MLP to model the vector field for all models. The generative points on the simplex and NLL are calculated using the Dopri5 ODE solver [9] and are shown in Fig.3.

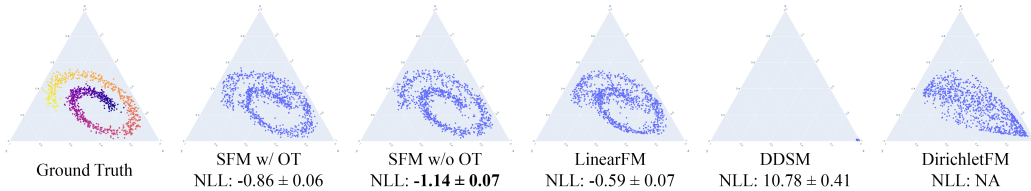


Figure 3: Generated samples of the Swill roll on simplex dataset and NLL (lower is better).

We note that most existing models assume the target data to be delta measures (one-hot distributions) and cannot be applied to this task. Both **DDSM** [7] and **DirichletFM** [56] imposed strong prior assumptions on the data distribution as Dirichlet distributions, which failed to capture the complex geometric shape of the Swill roll data points as demonstrated in the generated samples. On the contrary, directly built upon the geometry of the statistical manifold, our SFM model successfully captured the detailed data geometry. As no data resides on the boundary, exact NLL can be obtained using Eq.13 and was averaged over all points in the dataset. Though linear flow matching could also capture the geometry of the data, our SFM outperformed it in terms of NLL.

4.2 Binarized MNIST

We extend our SFM to model discrete generation tasks in computer vision. The binarized MNIST dataset [49] is the binarized version of the original MNIST dataset [33] by thresholding the original continuous value to be either 0 or 1, thus can be viewed as a 2-class generation task with a data dimension of $28^2 = 784$. We also compared **D3PM** [6] with an additional absorbing state. We used a convolutional neural net adopted from [53] with additional additive Fourier-based time embeddings. The quantitative evaluation of NLL and Fréchet inception distance (FID) are shown in Tab.1.

Table 1: NLL and FID of different discrete models on binarized MNIST. * is from [7].

	SFM w/ OT	SFM w/o OT	LinearFM	D3PM	DDSM	DirichletFM
NLL↓	-1.687 ± 0.020	-1.631 ± 0.027	0.622 ± 0.022	0.141 ± 0.021	0.100 ± 0.001*	NA
FID↓	4.62	5.15	5.91	10.35	7.79	40.60

All the generated results and NLL calculations were based on the Dopri5 ODE solver. Additional ablation results can be found in Appendix D.1 and generated images can be found in Appendix D.2. The NLL for diffusion-based models (D3PM and DDSM) was also calculated based on the variational bounds derived in their papers. Our proposed model consistently outperformed both the linear flow matching and other diffusion baselines in terms of FID and NLL, achieving higher sample quality and likelihood.

4.3 Text8

The Text8 dataset [39] is a media-size character-level corpus consisting of a small vocabulary of 27, which includes 26 lowercase letters and the whitespace token. We followed the convention in previous work [6, 23] to use random chunks of length 256 in both training and evaluation without any preprocessing. We used a 12-layer transformer-based predictor modified from [47] with additional time embeddings. As our exact likelihood is not directly comparable to bits-per-character (BPC) reported in previous work, we additionally calculated the pseudo-BPC inspired by [50]. See Appendix B.2 for additional details. All generated samples and NLL were estimated using 256 Euler steps. Quantitative results of BPC and NLL are provided in Tab.2 and generated texts are provided in Appendix D.2. The results for the transformer-based autoregressive language models are also provided as a reference. Our proposed SFM achieved the second-best performance among all diffusion or flow baselines. We also noted a significant performance gap between SFM and the naive linear flow matching on simplex, which highlighted the importance of capturing the intrinsic geometric properties of the underlying statistical manifold. Optimal transport does not significantly affect the final performance here, which we presume might be due to the long training stage in which vector fields were well-explored.

Table 2: BPC and NLL of different models on Text8. Results marked * are taken from corresponding papers.

Model	BPC↓ / (NLL↓)
SFM w/ OT	1.291 (-0.776 ± 0.114)
SFM w/o OT	1.298 (-0.856 ± 0.132)
LinearFM	1.935 (25.834 ± 0.186)
D3PM-absorb	1.47*
BFN[23]	1.41*
SEDD-absorb[37]	1.32*
Discrete Flow[59]	1.23*
Argmax Flow[27]	1.80*
Transformer[6]	1.23*
Transformer XL[17]	1.08*

Table 3: SP-MSE on the generated promoter DNA sequences. * are from [7] and † are from [56].

Model	SP-MSE↓
SFM w/ OT	0.0279
SFM w/o OT	0.0258
LinearFM	0.0282
DDSM	0.0334*
D3PM-uniform	0.0375*
Bit-Diffusion (one-hot) [16]	0.0395*
Bit-Diffusion (bit) [16]	0.0414*
Language Model	0.0333†
DirichletFM	0.0269†

4.4 Promoter Design

We further apply SFM to the practical task of promoter DNA sequence design in the bioinformatics realm. The promoter is a key element in gene transcription and regulation, and the generation of desired promoters can better help us understand the intricate interactions between human genes. [7] proposed a human promoter sequence dataset containing 100k promoter sequences with the corresponding transcription initiation signal profiles. Each promoter sequence is 1024 base pairs long and is centered at the annotated transcription start site position [26]. Therefore, we can model promoter design as a generation task with 4 categories (the base pair ATGC) conditioned on the given transcription signals. We follow [7] to concatenate the signal as additional input to the vector field predictor built upon 20 stacks of 1-dimensional convolutional layers on the input sequence. Optimal transport can also be applied for conditional generation, as we can pair the conditions with the input to make sure that the conditional arguments align with the target one-hot distributions.

To provide a quantitative evaluation of the generated promoter sequences, we follow [7] to apply the pre-trained deep learning sequence model Sei [14] to predict active promoters based on predictions of the chromatin mark H3K4me3. As the dataset spans the whole range of human promoter activity levels from highly expressed promoters to those with very low expression, the evaluation is based on comparing the scores between the generated sequences and the ground truth human genome promoter sequences on the test chromosomes. The metric SP-MSE is the mean squared error between the predicted promoter activity of the generated sequences and human genome sequences (lower is better) and is demonstrated in Tab.3. Our SFM was able to achieve the lowest SP-MSE score compared with other baselines. It is worth noting, though, that optimal transport produced slightly sub-optimal results. We hypothesize that this is because, in conditional generative tasks, the final generation should rely heavily on the conditions. Simply matching inputs with the targets using

distance measures may discard important information in the conditional arguments and may not be the best practice.

5 Related Work

As we put a special interest in discrete generation, we start with the existing work on discrete generation. We first list a few traditional autoregressive models [17, 47, 59] and masked language models [19, 50] but will skip them as we mainly focus on the diffusion and flow matching models. Existing diffusion and flow-based discrete generative models can be categorized into two main groups. The first group relies on stochastic jumps of Markov chains by treating discrete classes as Markov states. By choosing a proper transition matrix, the target one-hot distribution can be gradually noised into the stationary distribution. Noticeably, this approach can also adopt an additional absorbing state to mimic the mask token in masked language modeling [6]. D3PM [6] adapted the discrete-time Markov chain with the diffusion framework and SEDD [37] proposed a more efficient training scheme by learning the score entropy between different states. [12, 51] extended it to the continuous-time Markov chain by using the infinitesimal generator (rate matrix) instead, and [13] further applied the flow matching framework. Although the transition matrix or the rate matrix determines the entire diffusion trajectory, there is no canonical way of choosing it for different generation tasks to control the mixing rate. Also, due to the presence of discrete jumps of the Markov chain, exact likelihood calculation is no longer feasible. Only variational bounds were derived in [6, 13]. The other group directly works with the probability simplex or the logit space with certain assumptions of the underlying geometric structure. As an example, our linear flow matching assumes a Euclidean geometry on the probability simplex and is often used as a baseline in previous work [56]. The multinomial diffusion [27] assumed a Euclidean geometry on the logits space so interpolation became multiplication back on the probability simplex. Dirichlet diffusion (DDSM) [7] and Dirichlet flow matching (DirichletFM) [56] exerted a strong prior assumption on the probability path as the Jacobi diffusion process. We provide a more detailed analysis of these models in Appendix A.4. For models that directly operate on the logit space, the Bayesian flow network (BFN) assumed Gaussian distributions on the logit space with Bayesian update rules. [38] also assumed a Euclidean geometry in the logit space with targets as soft one-hot logits. The assumptions made in these models may not always hold, e.g., for the Swill roll on simplex dataset in Fig.3. These assumptions also did not necessarily capture the true geometry of the underlying statistical manifold. In contrast, our proposed SFM framework does not exert any strong prior assumptions and is aware of the intrinsic geometry by following the geodesics.

We also briefly review the related work on statistical manifolds and information geometry. The field of information geometry, the study of geometric properties of statistical manifolds, was first established in Rao’s seminal paper in 1945 [48] discussing the Fisher information metric. Most previous work utilizing information geometry focuses on optimization [2, 3] with a few exceptions on representation learning. [60] utilized the geodesic distance between two univariate Gaussians for function shape matching for retrosynthesis of gold nanoparticles. [34] treated point cloud data as probability measures over the 3D Euclidean space and considered the pullback metric on the latent space to obtain optimal latent coordinates for the autoencoder. [45] further applied such a method on single-cell RNA sequence trajectories. These models demonstrated the advantage of following the proper geometry compared with the vanilla Euclidean setting, but the pullback metric needed to be evaluated with expensive Jacobian-vector products during training. In contrast, our proposed SFM, for the first time, leverages mathematical tools from information geometry to generative modeling. SFM directly operates on the statistical manifold with closed-form geodesics, providing a simulation-free approach for efficient generative training.

6 Discussion

In this paper, we proposed statistical flow matching (SFM) as a general generative framework for generative modeling on the statistical manifold of probability measures. By leveraging results from information geometry, our SFM effectively captures the underlying intrinsic geometric properties of the statistical manifold. Specifically, we focused on the statistical manifold of categorical distributions in this work and derived optimal transport and exact likelihood formulae. We applied SFM to diverse downstream discrete generation tasks across different domains to demonstrate our framework’s

effectiveness over the baselines. We noted that SFM can be further extended to non-discrete generative tasks whose targets are probability distributions, which we will leave as future work.

We are also aware of the limitations of our SFM framework. As a special case of the flow matching model, the generation is an iterative process of refinement that cannot modify the size of the initial input. This may pose limitations to generation compared with autoregressive models. Furthermore, we adopted the assumption of independence between classes so that the canonical Riemannian structure can be induced by the Fisher metric. However, discretized data like CIFAR-10 [31] (256 ordinal pixel values) do not follow this assumption, and results on such data might be suboptimal.

References

- [1] S. Alamdari, N. Thakkar, R. van den Berg, A. X. Lu, N. Fusi, A. P. Amini, and K. K. Yang. Protein generation with evolutionary diffusion: sequence is all you need. *bioRxiv*, pages 2023–09, 2023.
- [2] S.-I. Amari. Natural gradient works efficiently in learning. *Neural computation*, 10(2):251–276, 1998.
- [3] S.-i. Amari and A. Cichocki. Adaptive blind signal processing-neural network approaches. *Proceedings of the IEEE*, 86(10):2026–2048, 1998.
- [4] S.-i. Amari and H. Nagaoka. *Methods of information geometry*, volume 191. American Mathematical Soc., 2000.
- [5] C. Atkinson and A. F. Mitchell. Rao’s distance measure. *Sankhyā: The Indian Journal of Statistics, Series A*, pages 345–365, 1981.
- [6] J. Austin, D. D. Johnson, J. Ho, D. Tarlow, and R. Van Den Berg. Structured denoising diffusion models in discrete state-spaces. *Advances in Neural Information Processing Systems*, 34:17981–17993, 2021.
- [7] P. Avdeyev, C. Shi, Y. Tan, K. Dudnyk, and J. Zhou. Dirichlet diffusion score model for biological sequence generation. In *International Conference on Machine Learning*, pages 1276–1301. PMLR, 2023.
- [8] N. Ay, J. Jost, H. Vân Lê, and L. Schwachhöfer. *Information geometry*, volume 64. Springer, 2017.
- [9] R. Bank, R. Graham, J. Stoer, and R. Varga. Springer series in 8. 1993.
- [10] H. Ben-Hamu, S. Cohen, J. Bose, B. Amos, A. Grover, M. Nickel, R. T. Chen, and Y. Lipman. Matching normalizing flows and probability paths on manifolds. *arXiv preprint arXiv:2207.04711*, 2022.
- [11] A. J. Bose, T. Akhound-Sadegh, K. Fatras, G. Huguet, J. Rector-Brooks, C.-H. Liu, A. C. Nica, M. Korablyov, M. Bronstein, and A. Tong. Se (3)-stochastic flow matching for protein backbone generation. *arXiv preprint arXiv:2310.02391*, 2023.
- [12] A. Campbell, J. Benton, V. De Bortoli, T. Rainforth, G. Deligiannidis, and A. Doucet. A continuous time framework for discrete denoising models. *Advances in Neural Information Processing Systems*, 35:28266–28279, 2022.
- [13] A. Campbell, J. Yim, R. Barzilay, T. Rainforth, and T. Jaakkola. Generative flows on discrete state-spaces: Enabling multimodal flows with applications to protein co-design. *arXiv preprint arXiv:2402.04997*, 2024.
- [14] K. M. Chen, A. K. Wong, O. G. Troyanskaya, and J. Zhou. A sequence-based global map of regulatory activity for deciphering human genetics. *Nature genetics*, 54(7):940–949, 2022.
- [15] R. T. Chen and Y. Lipman. Riemannian flow matching on general geometries. *arXiv preprint arXiv:2302.03660*, 2023.

- [16] T. Chen, R. Zhang, and G. Hinton. Analog bits: Generating discrete data using diffusion models with self-conditioning. *arXiv preprint arXiv:2208.04202*, 2022.
- [17] Z. Dai, Z. Yang, Y. Yang, J. Carbonell, Q. V. Le, and R. Salakhutdinov. Transformer-xl: Attentive language models beyond a fixed-length context. *arXiv preprint arXiv:1901.02860*, 2019.
- [18] Q. Dao, H. Phung, B. Nguyen, and A. Tran. Flow matching in latent space. *arXiv preprint arXiv:2307.08698*, 2023.
- [19] J. Devlin, M.-W. Chang, K. Lee, and K. Toutanova. Bert: Pre-training of deep bidirectional transformers for language understanding. *arXiv preprint arXiv:1810.04805*, 2018.
- [20] K. Fatras, Y. Zine, S. Majewski, R. Flamary, R. Gribonval, and N. Courty. Minibatch optimal transport distances; analysis and applications. *arXiv preprint arXiv:2101.01792*, 2021.
- [21] S. Gallot, D. Hulin, and J. Lafontaine. *Riemannian Geometry*. Universitext. Springer Berlin Heidelberg, 2004.
- [22] A. Graves. Generating sequences with recurrent neural networks. *arXiv preprint arXiv:1308.0850*, 2013.
- [23] A. Graves, R. K. Srivastava, T. Atkinson, and F. Gomez. Bayesian flow networks. *arXiv preprint arXiv:2308.07037*, 2023.
- [24] K. He, X. Zhang, S. Ren, and J. Sun. Deep residual learning for image recognition. In *Proceedings of the IEEE conference on computer vision and pattern recognition*, pages 770–778, 2016.
- [25] J. Ho, A. Jain, and P. Abbeel. Denoising diffusion probabilistic models. *Advances in neural information processing systems*, 33:6840–6851, 2020.
- [26] C.-C. Hon, J. A. Ramiłowski, J. Harshbarger, N. Bertin, O. J. Rackham, J. Gough, E. Denisenko, S. Schmeier, T. M. Poulsen, J. Severin, et al. An atlas of human long non-coding rnas with accurate 5' ends. *Nature*, 543(7644):199–204, 2017.
- [27] E. Hoogeboom, D. Nielsen, P. Jaini, P. Forré, and M. Welling. Argmax flows and multinomial diffusion: Learning categorical distributions. *Advances in Neural Information Processing Systems*, 34:12454–12465, 2021.
- [28] V. T. Hu, W. Zhang, M. Tang, P. Mettes, D. Zhao, and C. Snoek. Latent space editing in transformer-based flow matching. In *Proceedings of the AAAI Conference on Artificial Intelligence*, volume 38, pages 2247–2255, 2024.
- [29] M. F. Hutchinson. A stochastic estimator of the trace of the influence matrix for laplacian smoothing splines. *Communications in Statistics-Simulation and Computation*, 18(3):1059–1076, 1989.
- [30] L. Klein, A. Krämer, and F. Noé. Equivariant flow matching. *Advances in Neural Information Processing Systems*, 36, 2024.
- [31] A. Krizhevsky, G. Hinton, et al. Learning multiple layers of features from tiny images. 2009.
- [32] A. Le Brigant, S. C. Preston, and S. Puechmorel. Fisher-rao geometry of dirichlet distributions. *Differential Geometry and its Applications*, 74:101702, 2021.
- [33] Y. LeCun, C. Cortes, and C. Burges. Mnist handwritten digit database. *ATT Labs [Online]*. Available: <http://yann.lecun.com/exdb/mnist>, 2, 2010.
- [34] Y. Lee, S. Kim, J. Choi, and F. Park. A statistical manifold framework for point cloud data. In *International Conference on Machine Learning*, pages 12378–12402. PMLR, 2022.
- [35] G. Lin, A. Milan, C. Shen, and I. Reid. Refinenet: Multi-path refinement networks for high-resolution semantic segmentation. In *Proceedings of the IEEE conference on computer vision and pattern recognition*, pages 1925–1934, 2017.

- [36] Y. Lipman, R. T. Chen, H. Ben-Hamu, M. Nickel, and M. Le. Flow matching for generative modeling. *arXiv preprint arXiv:2210.02747*, 2022.
- [37] A. Lou, C. Meng, and S. Ermon. Discrete diffusion language modeling by estimating the ratios of the data distribution. *arXiv preprint arXiv:2310.16834*, 2023.
- [38] R. K. Mahabadi, J. Tae, H. Ivison, J. Henderson, I. Beltagy, M. E. Peters, and A. Cohan. Tess: Text-to-text self-conditioned simplex diffusion. *arXiv preprint arXiv:2305.08379*, 2023.
- [39] M. Mahoney. Large text compression benchmark, 2011.
- [40] J. Martens. New insights and perspectives on the natural gradient method. *Journal of Machine Learning Research*, 21(146):1–76, 2020.
- [41] E. Mathieu and M. Nickel. Riemannian continuous normalizing flows. *Advances in Neural Information Processing Systems*, 33:2503–2515, 2020.
- [42] H. K. Miyamoto, F. C. Meneghetti, and S. I. Costa. On closed-form expressions for the fisher-rao distance. *arXiv preprint arXiv:2304.14885*, 2023.
- [43] K. Nguyen, D. Nguyen, T. Pham, N. Ho, et al. Improving mini-batch optimal transport via partial transportation. In *International Conference on Machine Learning*, pages 16656–16690. PMLR, 2022.
- [44] L. Nurbekyan, W. Lei, and Y. Yang. Efficient natural gradient descent methods for large-scale pde-based optimization problems. *SIAM Journal on Scientific Computing*, 45(4):A1621–A1655, 2023.
- [45] A. Palma, S. Rybakov, L. Hetzel, and F. J. Theis. Modelling single-cell rna-seq trajectories on a flat statistical manifold. In *NeurIPS 2023 AI for Science Workshop*, 2023.
- [46] H. Park, S.-I. Amari, and K. Fukumizu. Adaptive natural gradient learning algorithms for various stochastic models. *Neural Networks*, 13(7):755–764, 2000.
- [47] A. Radford, J. Wu, R. Child, D. Luan, D. Amodei, I. Sutskever, et al. Language models are unsupervised multitask learners. *OpenAI blog*, 1(8):9, 2019.
- [48] C. R. Rao. Information and the accuracy attainable in the estimation of statistical parameters. In *Breakthroughs in Statistics: Foundations and basic theory*, pages 235–247. Springer, 1992.
- [49] R. Salakhutdinov and I. Murray. On the quantitative analysis of deep belief networks. In *Proceedings of the 25th international conference on Machine learning*, pages 872–879. ACM, 2008.
- [50] J. Salazar, D. Liang, T. Q. Nguyen, and K. Kirchhoff. Masked language model scoring. *arXiv preprint arXiv:1910.14659*, 2019.
- [51] J. E. Santos, Z. R. Fox, N. Lubbers, and Y. T. Lin. Blackout diffusion: generative diffusion models in discrete-state spaces. In *International Conference on Machine Learning*, pages 9034–9059. PMLR, 2023.
- [52] Y. Song and S. Ermon. Generative modeling by estimating gradients of the data distribution. *Advances in neural information processing systems*, 32, 2019.
- [53] Y. Song and S. Ermon. Improved techniques for training score-based generative models. *Advances in neural information processing systems*, 33:12438–12448, 2020.
- [54] Y. Song, J. Gong, M. Xu, Z. Cao, Y. Lan, S. Ermon, H. Zhou, and W.-Y. Ma. Equivariant flow matching with hybrid probability transport for 3d molecule generation. *Advances in Neural Information Processing Systems*, 36, 2024.
- [55] H. Stark, B. Jing, R. Barzilay, and T. Jaakkola. Harmonic prior self-conditioned flow matching for multi-ligand docking and binding site design. In *NeurIPS 2023 AI for Science Workshop*, 2023.

- [56] H. Stark, B. Jing, C. Wang, G. Corso, B. Berger, R. Barzilay, and T. Jaakkola. Dirichlet flow matching with applications to dna sequence design. *arXiv preprint arXiv:2402.05841*, 2024.
- [57] C. Szegedy, V. Vanhoucke, S. Ioffe, J. Shlens, and Z. Wojna. Rethinking the inception architecture for computer vision. In *Proceedings of the IEEE conference on computer vision and pattern recognition*, pages 2818–2826, 2016.
- [58] L. Theis, A. v. d. Oord, and M. Bethge. A note on the evaluation of generative models. *arXiv preprint arXiv:1511.01844*, 2015.
- [59] D. Tran, K. Vafa, K. Agrawal, L. Dinh, and B. Poole. Discrete flows: Invertible generative models of discrete data. *Advances in Neural Information Processing Systems*, 32, 2019.
- [60] K. Vaddi, H. T. Chiang, and L. D. Pozzo. Autonomous retrosynthesis of gold nanoparticles via spectral shape matching. *Digital Discovery*, 1(4):502–510, 2022.
- [61] A. Vaswani, N. Shazeer, N. Parmar, J. Uszkoreit, L. Jones, A. N. Gomez, Ł. Kaiser, and I. Polosukhin. Attention is all you need. *Advances in neural information processing systems*, 30, 2017.
- [62] J. Yim, A. Campbell, A. Y. Foong, M. Gastegger, J. Jiménez-Luna, S. Lewis, V. G. Satorras, B. S. Veeling, R. Barzilay, T. Jaakkola, et al. Fast protein backbone generation with se (3) flow matching. *arXiv preprint arXiv:2310.05297*, 2023.

Supplementary Material

A Riemannian Manifold and Information Geometry

In this section, we give a more detailed mathematical background on Riemannian manifold and information geometry related to this work. A more comprehensive background on the Riemannian manifold can be found in [21]. For information geometry, [8, 4] provide more comprehensive analyses and rigorous formulations.

A.1 Riemannian Manifold

A Riemannian manifold \mathcal{M} is a real, smooth manifold equipped with a positive definite inner product g on the tangent space $T_x(\mathcal{M})$ at each point $x \in \mathcal{M}$. Let $T\mathcal{M} = \bigcup_{x \in \mathcal{M}} T_x(\mathcal{M})$ be the *tangent bundle* of the manifold \mathcal{M} , a time-dependent *vector field* on \mathcal{M} is a mapping $u_t : [0, 1] \times \mathcal{M} \rightarrow T\mathcal{M}$ where $u_t(x) \in T_x(\mathcal{M})$. A *geodesic* is a locally distance-minimizing curve on the manifold. The existence and the uniqueness of the geodesic state that for any point $x \in \mathcal{M}$ and for any tangent vector $u \in T_x(\mathcal{M})$, there exists a unique geodesic $\gamma : [0, 1] \rightarrow \mathcal{M}$ such that $\gamma(0) = x$ and $\gamma'(0) = u$. The *exponential map* $\exp : \mathcal{M} \times T\mathcal{M} \rightarrow \mathcal{M}$ is uniquely defined to be $\exp_x(u) := \gamma(1)$. The *logarithm map* $\log : \mathcal{M} \times \mathcal{M} \rightarrow T\mathcal{M}$ is defined as the inverse mapping of the exponential map such that $\exp_x(\log_x(y)) \equiv y, \forall x, y \in \mathcal{M}$ ¹. With the exponential map and logarithm map, the time-dependent flow can be compactly written as time interpolation along the geodesic:

$$x_t := \psi_t(x_t|x_0, x_1) = \exp_{x_0}(t \log_{x_0} x_1), \quad t \in [0, 1] \quad (15)$$

It can be demonstrated that the above flow indeed traces the geodesic between x_0, x_1 with linearly decreasing geodesic distance $d_g(x_t, x_1) = (1-t)d_g(x_0, x_1)$ [15]. For an n -dimensional Riemannian manifold, the geodesic can be obtained by solving the geodesic equation

$$\sum_{j=1}^n g_{ji} \frac{d^2 x_j}{dt^2} + \sum_{j=1}^n \sum_{k=1}^n \Gamma_{ijk} \frac{dx_j}{dt} \frac{dx_k}{dt} = 0, \quad i = 1, 2, \dots, n \quad (16)$$

where x_i are local coordinates of the geodesic and Γ_{ijk} are the Christoffel symbols of the first kind defined by

$$\Gamma_{ijk} = \frac{1}{2} \left(\frac{\partial g_{ji}}{\partial x_k} + \frac{\partial g_{ji}}{\partial x_j} - \frac{\partial g_{jk}}{\partial x_i} \right), \quad i, j, k = 1, 2, \dots, n \quad (17)$$

The closed-form expressions for the geodesic are generally not available. [42] curated a wide range of common statistical manifolds for parameterized families of both the discrete and the continuous distributions. We will focus on the statistical manifold of categorical distributions and also the spherical manifold, as the latter is closely related to the former via the diffeomorphism π in Eq.(5).

A.2 Spherical Manifold

The positive orthant of the unit $(n-1)$ -sphere S_+^{n-1} is a $(n-1)$ -dimensional manifold. The sphere can be embedded into the ambient Euclidean manifold \mathbb{R}^n so it inherits the canonical inner product as

$$\langle u, v \rangle_S = \langle u, v \rangle = \sum_{i=1}^n u_i v_i, \quad u, v \in T_x(S_+^{n-1}) \quad (18)$$

The tangent space $T_x(S_+^{n-1}) = \{u | \langle u, x \rangle = 0\}$ is a $(n-1)$ -dimensional hyperplane perpendicular to the vector x . The geodesic on the sphere follows the great circle between two points, and the geodesic distance can be calculated in Eq.7. The corresponding exponential map can be calculated as:

$$\exp_x(u) = x \cos \|u\|_2 + u \operatorname{sinc} \|u\|_2 \quad (19)$$

where $\operatorname{sinc}(\theta) = \sin \theta / \theta$ is the unnormalized sinc function. The logarithm map can be calculated as:

$$\log_x(y) = \arccos(\langle x, y \rangle) \frac{P_x(y-x)}{\|P_x(y-x)\|_2} \quad (20)$$

where $P_x(w) = w - \langle x, w \rangle x$ is the projection of vector w onto the tangent space $T_x(S_+^{n-1})$.

¹Note that the formulation here is slightly different from Sec.2.1 where we fix a point μ on \mathcal{P} .

A.3 Statistical Manifold of Categorical Distributions

The statistical manifold of categorical distributions $\mathcal{P}(\mathcal{X})$ is closely related to S_+^{n-1} by the diffeomorphism π in Eq.(5). In fact, π is an isometry between the Fisher information metric on \mathcal{P} and the standard induced metric on S_+^{n-1} up to a constant scaling factor of 1/4. To see this, we have the following proposition:

Proposition 2.

$$\left\langle \frac{\partial \pi(\mu)}{\partial u}, \frac{\partial \pi(\mu)}{\partial v} \right\rangle = \frac{1}{4} \langle u, v \rangle_\mu, \quad u, v \in T_\mu(\mathcal{P}) \quad (21)$$

Proof.

$$\left\langle \frac{\partial \pi(\mu)}{\partial u}, \frac{\partial \pi(\mu)}{\partial v} \right\rangle = \left\langle \frac{d}{dt} \pi(\mu + tu) \Big|_{t=0}, \frac{d}{dt} \pi(\mu + tv) \Big|_{t=0} \right\rangle = \sum_{i=1}^n \frac{u_i}{2\sqrt{\mu_i}} \frac{v_i}{2\sqrt{\mu_i}} = \frac{1}{4} \langle u, v \rangle_\mu$$

□

Note that the infinitesimal arc length on the geodesic can be expressed as $ds^2 = \|dx\|_g^2 = \sum_{j,k} dx_j g_{jk}(x) dx_k$ where $\|\cdot\|_g$ is the canonical Riemannian norm induced by the inner product. Integrating over the geodesic, we can easily arrive at the result in Proposition 1. Based on this, the exponential map and logarithm map on this statistical manifold can be written as

$$\exp_\mu(u) = \left(\sqrt{\mu} \cos \left\| \frac{u}{2\sqrt{\mu}} \right\|_2 + \frac{u}{2\sqrt{\mu}} \operatorname{sinc} \left\| \frac{u}{2\sqrt{\mu}} \right\|_2 \right)^2 \quad (22)$$

$$\log_\mu(\nu) = \frac{2 \arccos(\langle \sqrt{\mu}, \sqrt{\nu} \rangle)}{\sqrt{1 - \langle \sqrt{\mu}, \sqrt{\nu} \rangle}} (\sqrt{\mu} \odot \nu - \langle \sqrt{\mu}, \sqrt{\nu} \rangle \mu) \quad (23)$$

where \odot denotes the pairwise multiplication. We mentioned in the main text that directly using the exponential and logarithm maps on the statistical manifold has numerical issues near the boundary. Instead, we used the mapping π to work with the spherical manifold. Nonetheless, Eq.(22) and (23) provide useful tools for visualization of the statistical manifold, as demonstrated in Fig.1.

We also noted the relation between the Fisher information metric defined in Eq.1 and the canonical inner product defined in Eq.4 for general statistical manifolds. Let \mathcal{M} be an n -dimensional differentiable manifold and consider an embedding defined by $\mathcal{M} \hookrightarrow \mathcal{P}(\mathcal{M}), \theta \mapsto p(\theta) = \sum_{i \in \mathcal{X}} p_i(\theta) \delta^i$. The pullback of the Fisher metric g defines a metric on \mathcal{M} . For $u, v \in T_\theta(\mathcal{M})$, we have

$$\begin{aligned} g_\theta(u, v) &:= p^*(g)_\theta(u, v) \\ &= g_{p(\theta)} \left(\frac{\partial p}{\partial u}, \frac{\partial p}{\partial v} \right) \\ &= \sum_i \frac{1}{p_i(\theta)} \frac{\partial p_i}{\partial u}(\theta) \frac{\partial p_i}{\partial v}(\theta) \\ &= \sum_i p_i(\theta) \frac{\partial \log p_i}{\partial u}(\theta) \frac{\partial \log p_i}{\partial v}(\theta) \end{aligned} \quad (24)$$

which gives the more common definition of the Fisher information matrix in Eq.1. This relation also generally holds for a continuous sample space \mathcal{X} but requires more careful handling with measure theory tools. We refer interested readers to mathematical references, e.g., Chapter 3.1 in [8].

A.4 Other Statistical Manifolds

The statistical manifold of categorical distributions provides an intuitive way of modeling discrete targets. However, we noted that other parameterized distributions can also be used to derive alternative statistical manifolds with different geometries. We will briefly discuss some manifolds that have been used in previous generative models (though not from the information geometry perspective as we do).

Dirichlet Distribution The Dirichlet distribution $\text{Dir}(\alpha)$ is a multivariate generalization of the beta distribution. It is defined on the $(n - 1)$ -dimensional simplex Δ^{n-1} with n concentration parameters $\alpha = \{\alpha_i\}_{i=1}^n$. The probability density function is defined as

$$p(x; \alpha) = \frac{1}{B(\alpha)} \prod_{i=1}^n x_i^{\alpha_i - 1}, \quad x \in \Delta^{n-1} \quad (25)$$

where $B(\alpha) = \prod_{i=1}^n \Gamma(\alpha_i) / \Gamma(\sum_{i=1}^n \alpha_i)$ is the multivariate beta function. The closed-form expressions for the geodesics between Dirichlet distributions (and for the marginal beta distributions, as were used in [7]) are unknown. It is known that, however, this statistical manifold has non-constant negative sectional curvatures everywhere [32]. [7] proposed to follow the specific path of Jacobi diffusion processes on the marginal beta distributions, for which expensive modified Jacobi polynomials needed to be precomputed. [56] further applied the flow matching framework by considering the probability path of $\text{Dir}(1 + te_k)$ for some fixed maximum timestep. Still, expensive calculations of the regularized incomplete beta functions were required. Compared with these two generative models, our proposed SFM on categorical distributions has the following advantages:

- DDSM and DirichletFM have strong prior assumptions that the categorical distributions follow some specific forward noising process which always terminates at (or near) one-hot distributions. This assumption generally holds for discrete generation, but cannot be generalized to more complex geometry on the probability simplex, as we have demonstrated in our toy example of the Swill roll on simplex dataset in Fig.3.
- The forward noising paths are not the shortest geodesics in the sense of the Riemannian metric. In our SFM, the vector fields always follow the geodesic, thus following the sharpest direction of decreasing KL divergence (see Sec.3.3).
- Our SFM framework does not require the computation of expensive polynomials and is more mathematically concise.
- The final one-hot distributions are unreachable in [56], as it would require an infinite timestep. Therefore, a variational bound needs to be derived for likelihood estimation, which was not done in the original paper.

Multinomial Distribution Consider m i.i.d. experiments that follow a categorical distribution with n possible outcomes and probability $\mu = \{\mu_i\}_{i=1}^n$, a multinomial distribution gives the probability of getting x_i times the i -th outcome with $\sum_{i=1}^n x_i = m$. The geodesic distance for multinomial distributions is identical to that of the categorical distributions up to a scaling constant [42]:

$$d_{\text{mul}}(\mu, \nu) = \sqrt{n} d_{\text{cat}}(\mu, \nu) = 2\sqrt{n} \arccos \left(\sum_{i=1}^n \sqrt{\mu_i \nu_i} \right) \quad (26)$$

Therefore, our model can also be interpreted as multinomial flow matching on the corresponding statistical manifold. The previous work of multinomial diffusion (argmax flow) [27] transformed the one-hot distribution to $ne_k - 1$ in the logit space (soft one-hot logits) and assumed the common Euclidean structure of the logit space for constructing the diffusion process. This assumption did not consider the intrinsic geometry of the underlying statistical manifold and also had the inaccessibility issue of the delta measure as DirichletFM. We have demonstrated that SFM consistently outperformed the naive multinomial diffusion on the Text8 datasets, indicating the effectiveness of tracing the true geodesics.

B Likelihood Calculation

In this section, we provide more concrete mathematical details regarding the exact likelihood calculation in the main text. We first make a distinction between negative log-likelihood (NLL) and bits-per-dimension (BPD, including bits-per-character, BPC) in this work. As we are dealing with probability distributions over the statistical manifold of probability measures, it is important for us to keep the difference between the probability spaces $\mathcal{P}(\mathcal{P}(\mathcal{X}))$ and $\mathcal{P}(\mathcal{X})$. In our notation, we use μ, ν to denote elements in $\mathcal{P}(\mathcal{X})$, or categorical distributions, and use p, q to denote elements in $\mathcal{P}(\mathcal{P}(\mathcal{X}))$, or distributions over categorical distributions. We further use NLL to refer to $-\log p(\mu)$ for a specific μ and BPD for categorical likelihood $-\log_2 p(\delta|\mu)$ where δ is the ground truth delta measure (one-hot

distribution). Note this definition of BPD (BPC) follows the convention in autoregressive language models where the conditional probabilities for the next token are calculated and averaged [17, 22]. In contrast, most previous work drew equivalence between these two concepts.

B.1 Negative Log-Likelihood (NLL) Calculation

Our SFM framework enjoys the exact negative log-likelihood calculation as a continuous normalizing flow model [36, 15]. It is worth noting that negative NLLs are not uncommon [15]. As a probability density, the NLL can indeed go to negative infinity at the boundary. Consider the arcsine distribution defined on the finite support $[0, 1]$ with the probability density function

$$p(\theta) = \frac{1}{\pi\sqrt{\theta(1-\theta)}}, \quad \theta \in (0, 1) \quad (27)$$

It is easy to see the density approaches infinity as θ approaches 0 or 1. Note that the arcsine distribution is a special case of beta distribution $\text{Beta}(\frac{1}{2}, \frac{1}{2})$, which is in turn a special case of Dirichlet distribution $\text{Dir}(\frac{1}{2}, \frac{1}{2})$. Each θ can be naturally viewed as the parameter for the Bernoulli distribution (2-class categorical distribution), so the arcsine distribution indeed defines a distribution over Bernoulli distributions with negative NLLs near the boundary. In fact, for discrete data, the target data always come in as delta measures, which indicates that the target distribution must be a convex combination of delta measures with infinite likelihood: $q = \sum_{i=1}^n \theta_i \delta_i$ where $\delta_i := \delta_{\delta^i}$ is the delta measure over the underlying delta measure δ^i on the discrete class i .

Variational Bound We followed [7] to derive a variational bound as marginalized over a small neighborhood of the delta measure in Eq.14 to obtain finite NLLs. The variational bound can be derived via the standard variational approach as

$$\begin{aligned} \log p(\delta) &= \mathbb{E}_{q(\mu|\delta)} [\log p(\delta)] \\ &= \mathbb{E}_{q(\mu|\delta)} \left[\log \left(\frac{p(\delta, \mu)}{p(\mu|\delta)} \right) \right] \\ &= \mathbb{E}_{q(\mu|\delta)} \left[\log \left(\frac{p(\delta, \mu) q(\delta, \mu)}{q(\mu|\delta) p(\mu|\delta)} \right) \right] \\ &= \mathbb{E}_{q(\mu|\delta)} \left[\log \left(\frac{p(\delta, \mu)}{q(\mu|\delta)} \right) \right] + D_{\text{KL}}(q(\mu|\delta) \| p(\mu|\delta)) \\ &\geq \mathbb{E}_{q(\mu|\delta)} \left[\log \left(\frac{p(\delta, \mu)}{q(\mu|\delta)} \right) \right] \\ &= \mathbb{E}_{q(\mu|\delta)} [\log p(\delta|\mu) + \log p(\mu) - \log q(\mu|\delta)] \end{aligned} \quad (28)$$

The posterior probability $q(\mu|\delta)$ serves as the forward diffusion process in [6, 56] with a closed-form expression that depends on the timestep. In our Riemannian flow matching formulation, however, such a forward process is implicitly defined via the time-interpolation along the geodesics. Nonetheless, we do know that the conditional distribution should approach the delta measure when $t \rightarrow 1$ as the geodesic distance approaches 0: $p_1(\mu|\delta) \approx \delta$. Therefore, as we are marginalized over a small neighborhood, we can define a time-dependent posterior distribution $q_t(\mu|\delta)$ that approaches δ as $t \rightarrow 1$. In principle, any forward probability that approaches the delta measure at $t = 1$ with an analytical likelihood can be used to derive the lower bound. For example, we can follow [7] to use the Jacobi diffusion process. To avoid the need for expensive Jacobi polynomial calculation, we instead use simple indicator measures over the simplex as

$$q_t(\mu|\delta^k) = \begin{cases} \frac{p_0}{(1-t)^{n-1}}, & \mu_i \leq t, 1 \leq i \leq n, i \neq k \\ 0, & \text{otherwise} \end{cases} \quad (29)$$

where p_0 is the base probability of the uniform distribution over the simplex, $\mu_i = \theta_i$ is the i -th component of the categorical distribution of μ . In other words, $q_t(\mu|\delta^k)$ is the time-interpolated probability between the delta measure and the uniform distribution: $q_t(\mu|\delta^k) = t\delta_k + (1-t)U\Delta^{n-1}$. We have

$$\log q_t(\mu|\delta^k) = \log p_0 - (n-1) \log(1-t) \quad (30)$$

In practice, we use $t = 0.995$ and provide more results in the ablation studies in Appendix D.1. The categorical likelihood $p(\delta^k|\mu)$ is the standard cross-entropy loss, also referred to as the *reconstruction loss* in some previous work [23]. It can be calculated as

$$\log p(\delta^k|\mu) = \log \mu_k \quad (31)$$

Prior Likelihood The prior likelihood accounts for the base probability when we sample from the prior noise distribution. During both the training and the inference stages, we uniformly sample from the simplex Δ^{n-1} . This can be efficiently done by normalizing n i.i.d random variables from the exponential distribution:

$$\tilde{\theta}_i \sim \text{Exp}(1), \theta_i = \tilde{\theta}_i / \sum_{k=1}^n \tilde{\theta}_k, \quad i = 1, 2, \dots, n \quad (32)$$

The uniform distribution over simplex is exactly the Dirichlet distribution $\text{Dir}(1, \dots, 1)$. Therefore, the log-likelihood can be calculated as

$$\log p_0 = -\log \Gamma(n) \quad (33)$$

where Γ is the Gamma function. Note that the prior likelihood is independent of the samples.

Change of Measure The diffeomorphism π in Eq.5 induces a push-forward measure on S_+^{n-1} which can be described by the change of measure identity

$$\pi_* p(\pi(\mu)) |\det d\pi(\mu)| = p(x), x = \pi(\mu) \quad (34)$$

The change of measure term can be calculated using the change of volume formula with the canonical coordinates $\{\tilde{x}_i\}_{i=1}^{n-1}$ and $\{\varphi_i\}_{i=1}^{n-1}$ as

$$\begin{aligned} \mu_1 &= \tilde{x}_1, & x_1 &= \cos \varphi_1 \\ \mu_2 &= \tilde{x}_2, & x_2 &= \sin \varphi_1 \cos \varphi_2 \\ &\vdots & &\vdots \\ \mu_{n-1} &= \tilde{x}_{n-1}, & x_{n-1} &= \sin \varphi_1 \dots \sin \varphi_{n-2} \cos \varphi_{n-1} \end{aligned} \quad (35)$$

where $0 \leq \varphi_i \leq \pi/2$. The diffeomorphism $x = \pi(\mu)$ is given by

$$\begin{aligned} \tilde{x}_1 &= \cos^2 \varphi_1 \\ \tilde{x}_2 &= \sin^2 \varphi_1 \cos^2 \varphi_2 \\ &\vdots \\ \tilde{x}_{n-1} &= \sin^2 \varphi_1 \dots \sin^2 \varphi_{n-2} \cos^2 \varphi_{n-1} \end{aligned} \quad (36)$$

The change of measure term is

$$\log |\det d\pi^{-1}(x)| = -(n-1) \log 2 - \sum_{i=1}^n \log x_i \quad (37)$$

Similarly, for the inverse mapping, the term is

$$\log |\det d\pi(\mu)| = (n-1) \log 2 + \frac{1}{2} \sum_{i=1}^n \log \mu_i \quad (38)$$

Model Likelihood The model likelihood can be viewed as the push-forward measure of the learned flow:

$$p_t = (\psi_t)_* p_0 \quad (39)$$

We demonstrated in Sec.3.5 that this term can be calculated as the integral of divergence in Eq.(12) plus the base probability in Eq.(33). More specifically, the NLL can be obtained as the solution to the following ODE system back through time with the initial condition of x_1 and $\log p_1^{\text{ODE}} = 0$:

$$\frac{d}{dt} \begin{bmatrix} x_t \\ \log p_t^{\text{ODE}} \end{bmatrix} = \begin{bmatrix} v_t(x_t) \\ -\text{div}_g(v_t)(x_t) \end{bmatrix} \quad (40)$$

For manifolds that can be embedded in the ambient Euclidean space (e.g., simplex and sphere), the Riemannian divergence can be calculated as the normal Euclidean divergence $\text{div}_g = \text{div}$ [15]. We further use Hutchinson’s trace estimator [29] to efficiently estimate the divergence as

$$\text{div } v_t(x) = \mathbb{E}_{\varepsilon \sim \mathcal{N}(0, I)}[\varepsilon^\top \nabla v_t(x) \varepsilon] \quad (41)$$

The expectation can be efficiently computed using the vector-Jacobian product.

Combining Eq.(30), (31), (33), (37), (38) with Eq.(14) and (13), we can efficiently calculate the NLL given arbitrary delta measures as input. The NLL calculation scheme is visualized in Fig.2 and described in Alg.1.

Algorithm 1 NLL Calculation for Discrete Data

- 1: Sample $\tilde{\mu}_1 \sim q_t(\mu|\delta)$ in Eq.(29) and calculate $-\log q_t(\tilde{\mu}_1|\delta)$ and $\log p(\delta|\tilde{\mu}_1)$.
 - 2: Apply the diffeomorphism in Eq.5 to obtain $\tilde{x}_1 = \pi(\tilde{\mu}_1)$ and calculate $\log |\det d\pi^{-1}(\tilde{x}_1)|$.
 - 3: Solve the ODE system in Eq.(40) to obtain x_0 and $\log p^{\text{ODE}}$.
 - 4: Apply π^{-1} to obtain $\mu_0 = \pi^{-1}(x_0)$ and calculate $\log |\det d\pi(\mu_0)|$.
 - 5: Calculate the base log probability $\log p_0(\mu_0)$.
 - 6: **return** NLL as in Eq.(14).
-

B.2 Bits-Per-Character (BPC) Calculation

We have demonstrated that the NLL can reach negative infinity. In contrast, in our definition of BPC with the cross-entropy loss $-\log_2 p(\delta|\mu)$, it is always non-negative and consistent with previous autoregressive language models. However, as our flow-based model is not autoregressive, we instead follow [50] to calculate the pseudo-NLL/BPC for comparison. The pseudo-log-likelihood of a D -dimensional data is defined as

$$\frac{1}{D} \sum_{d=1}^D \log p(x^d|x^{-d}) \quad (42)$$

where $x^{-d} = \{x^k, 1 \leq k \leq D, k \neq d\}$ represents the data without the specific dimension index d . BPC can be similarly defined as $-\frac{1}{d} \sum_{d=1}^D \log_2 p(x^d|x^{-d})$. In our evaluation with Text8, we always pick the middle token with a window of 128 known tokens before and 127 known tokens after. The model tries to recover the missing token given the conditional context. As our model only accepts one timestep for all data dimensions, instead of fixing the context, we still uniformly randomly sample all the initial noises from the simplex but substitute the corresponding vector fields with the ground truth ones to make sure the context tokens converge to the ground truth one-hot distributions.

C Experimental Setup

In this section, we further describe the experimental setup, model architecture, and datasets.

C.1 Model Parameterization

Our SFM architecture is encoder-agnostic and can be applied to arbitrary discrete generative tasks. Here, we describe the common setting of the flow model across different datasets. We use the sinusoidal timestep embedding described in [61] as $\text{Emb} : [0, 1] \rightarrow \mathbb{R}^H$. We follow [15] to manually project the predicted vector field onto the corresponding tangent space. For the spherical manifold, the projection can be described as

$$v_t(x_t) = \tilde{v}_t(x_t) - \langle x_t, \tilde{v}_t(x_t) \rangle x_t \quad (43)$$

For linear flow matching on the simplex, the projection can be described as

$$v_t(x_t) = \tilde{v}_t(x_t) - \frac{1}{n} \sum_{i=1}^n \tilde{v}_t(x_t)_i \quad (44)$$

The projection guarantees that the final prediction lies on the corresponding tangent space, and the data points will stay on the manifold during Euler sampling. We will always assume the projection

is performed in the following context of using v_t . The training stage of SFM is described in Alg.2. The time complexity of our SFM framework is dominated by the underlying vector field predictor with little overhead. Each model for binarized MNIST and promoter design was trained on a single NVIDIA A100 GPU for 6-10 hours. Each model for Text8 was trained on 8 NVIDIA A100 GPUs for about 7 days. We will further describe the encoders for each generation task in the following subsections.

Algorithm 2 Training SFM

```

1: while not converged do
2:   Sample noise distribution  $\mu_0 \sim p_0(\mu)$  and target distribution  $\mu_1 \sim q(\mu)$ .
3:   if optimal transport then
4:     Do batch OT assignments of  $\mu_0$  and  $\mu_1$  according to the average statistical distances.
5:   end if
6:   Apply the diffeomorphism in Eq.5 to obtain  $x_0 = \pi(\mu_0), x_1 = \pi(\mu_1)$ .
7:   Sample  $t \sim U[0, 1]$  and interpolate  $x_t = \exp_{x_0}(t \log_{x_0} x_1)$  using Eq.(19) and (20).
8:   Calculate the conditional vector field  $u_t^S(x_t|x_0, x_1) = \frac{d}{dt}x_t = \log_{x_t}(x_1)/(1-t)$ .
9:   Predict the vector field using  $v(x_t, t)$  and optimize the SFM loss in Eq.(8).
10: end while

```

C.2 Model Sampling

The sampling process from the trained model can be described as solving the differential equation $\frac{\partial}{\partial t}x_t = v_t(x_t)$ from $t = 0$ to 1 with the initial conditional x_0 sampled from the prior noise distribution. Alternatively, we can write the solution as the integral of the learned time-dependent vector through time as

$$x_1 = x_0 + \int_0^1 v_t(x_t)dt \quad (45)$$

We always use the Dopri5 ODE solver [9] for our ODE sampling and NLL calculation. For Euler method with N discrete steps, the timesteps $0, 1/N, 2/N, \dots, (N-1)/N$ are used with a step size of $1/N$. The sampling stage is described in Alg.3.

Algorithm 3 Sampling from SFM

```

1: Sample noise distribution  $\mu_0 \sim p_0(\mu)$ .
2: Apply the diffeomorphism in Eq.5 to obtain  $x_0 = \pi(\mu_0)$ .
3: if ODE sampling then
4:   Solve  $\frac{\partial}{\partial t}x_t = v_t(x_t)$  using Dopri5 ODE solver with initial condition  $x_0$ .
5: else ▷ Euler method
6:   for  $t \leftarrow 0, 1/N, 2/N, \dots, (N-1)/N$  do
7:      $x_{t+1/N} = \exp_{x_t}(v(x_t, t)/N)$ 
8:   end for
9: end if
10: return  $\mu_1 = \pi^{-1}(x_1)$ 

```

C.3 Swill Roll

The Swill roll on the 2-simplex is generated by normalizing the span of the 2-dimensional Swill roll to $[0 + \varepsilon, 1 - \varepsilon]$ where ε is a small margin to make sure no point lies on the boundary. The third dimensional is automatically obtained as $\mu_3 = 1 - \mu_1 - \mu_2$. We fixed a random seed and generated 1000 samples for a full batch training. The vector field predictor is based on simple multi-layer perceptions (MLPs) and can be described as

$$v(x_t, t) = \text{MLP}(\text{MLP}(x_t) \parallel \text{MLP}(\text{Emb}(t))) \quad (46)$$

where \parallel denotes concatenation and we used a hidden dimension of $H = 128$. Each model was trained for 2000 epochs using full batch gradient descent with an initial learning rate of 10^{-3} . 1000 samples were sampled using the Dopri5 ODE solver, and NLL was calculated on the whole data samples with 20 repeats. The DirichletFM model was originally trained with cross-entropy loss which could not be

used for this task. We instead used the binary cross-entropy loss during training and kept all the other flow-based part the same as described in the original paper [56].

C.4 Binarized MNIST

We used the preprocessed binarized MNIST dataset from [49] which has a split of 50k/10k/10k. We adopted the CNN-based vector field predictor from [53] with additional additive time embeddings at each convolution layer’s output. The model has 4 residual layers [24] and 4 refinement layers [35] with a total number of 29.8M trainable parameters. All models were trained for 100k iterations with a batch size of 256 (approximately 510 epochs) with an initial learning rate of 3×10^{-4} .

For the quantitative evaluation of the generated samples, we calculated the FID score for 1000 generated samples for each model. The statistics for the binarized MNIST dataset were calculated on the whole training set via the pre-trained InceptionV3 [57] model. The NLLs reported in the main text were calculated on a fixed subset with 1000 samples of the test set using the Dopri5 ODE solver.

C.5 Text8

We followed previous work [23, 6] to use a fixed split of 90M/5M/5M with a fixed sequence length of 256. We used a 12-layer transformer-based model modified from [47] with an additional additive time embedding. The resultant model has 85.1M trainable parameters. Noticeably, our model size is smaller than [23] which used a full 24-layer model, but is similar to [37]. The models were trained for 1M iterations with a batch size of 512 (approximately 23 epochs), an initial learning rate of 10^{-4} , and an exponential moving average (EMA) decay rate of 0.9999. We further used 1000 iterations as the linear warmup of the learning rate and used a decay rate of 0.8 with a patience of 3 and a validation interval of 2000 training iterations. The model snapshot with the lowest validation loss was saved for evaluation. BPC and NLL were calculated on the first 10k characters of the test set with 256 Euler steps, and generated texts were obtained using either 256 Euler steps or the Dopri5 ODE solver (see Appendix D.2).

C.6 Promoter Design

We used the splits from the dataset paper [7] that assign Chromosome 10 to the validation set, Chromosomes 8 and 9 to the test set, and all the other 21 human chromosomes to the training set. This assignment can avoid potential data leakage on the same chromosome. The transcription signals are provided as a float number for each base pair position. We also followed [7] to use a total number of 100k sequences with a context window of 1024 base pairs and added a random offset of 10 to the sequence position during training. The vector field predictor we used was identical to that in [7], with 20 stacks of 1D convolutional layers and a total number of 13.3M trainable parameters. Our models were trained for 200k iterations with a batch size of 256 and an initial learning rate of 5×10^{-4} . The model snapshot with the lowest validation SP-MSE on the validation set was saved for evaluation. The test SP-MSE was evaluated on the generated samples on the full test set’s transcription signals with 300 Euler steps of generation.

D Additional Result

In this section, we provide additional results of ablation studies as well as generated samples for each task.

D.1 Ablation Study

We provide ablation studies of the effect of different sampling methods, different sampling steps for the Euler methods, and different $t_{\max} \approx 1$ for NLL calculation. The results are provided in Tab.4. The effect of the variational timestep t_{\max} matched the results from [7], which stated that a closer timestep to the target data would decrease the NLL. The reasons we choose $t = 0.995$ instead of higher values are: 1) we noticed numerical stability issues at a timestep very close to the target, 2) we want a fair comparison with [7] which used an equivalent timestep of 0.9975, and 3) as long as we use a same timestep, the results are comparable within. We also found that NLL increased with the number of Euler sampling steps. We hypothesize that it is due to the large divergence change at $t \approx 1$

and naive Euler steps tend to overestimate its contribution. Nonetheless, the Euler method with more than 300 steps gave a similar NLL as the ODE solver. We further provide additional results of the FID scores on different sample methods in Tab.5 in which we used $t = 0.995$ and 300 Euler steps. The final performance was quite similar between these two sampling methods.

Table 4: NLL for different sampling methods, sampling steps, and t_{\max} .

Method	#step	t_{\max}	NLL↓
Euler	300	0.9995	-2.545 ± 0.029
		0.999	-2.442 ± 0.018
		0.995	-1.689 ± 0.031
		0.99	-1.019 ± 0.032
	100	-	-1.871 ± 0.020
	500	0.995	-1.677 ± 0.022
	1000	-	-1.647 ± 0.024
ODE	-	0.995	-1.687 ± 0.020

Table 5: FID for different sampling methods with $t_{\max} = 0.995$. For the Euler method, we used 300 steps.

Method	Model	FID↓
ODE	SFM w/ OT	-1.687 ± 0.020
	SFM w/o OT	-1.631 ± 0.027
	LinearFM	0.622 ± 0.022
Euler	SFM w/ OT	-1.689 ± 0.031
	SFM w/o OT	-1.653 ± 0.028
	LinearFM	0.499 ± 0.022

D.2 Generated Samples

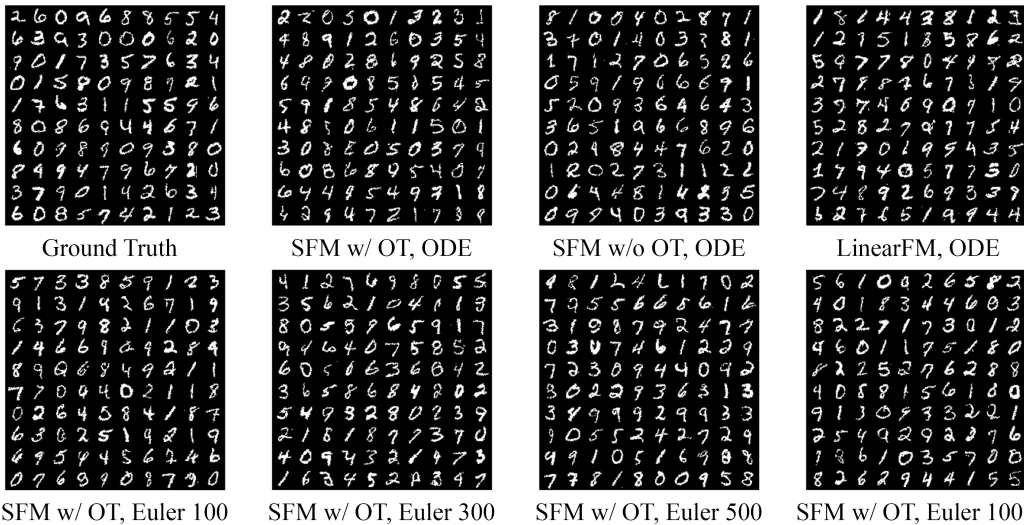


Figure 4: Generated samples of the binarized MNIST dataset from various models and different sampling settings.

The ground truth images and generated samples of the binarized MNIST dataset using various models and different sampling settings are demonstrated in Fig.4. The lower row demonstrates generated samples with different numbers of Euler steps. Generated texts on the Text8 dataset using different models and sampling methods are demonstrated below.

SFM w/ OT, ODE

a_gull_a_clock_as_sing_cowbreaks_diseases_in_forms_the_eilewes_of_clocks_contained_four_two_scarters_to_be_cursed_norse_the_hygg
y_alnanking_wade_of_joul_veine_in_one_ovias_sn_gl_cz_asi_evic_hal_art_diseashe_the_final_cangent_oedesis_spurl_the_last_one_surf
_cut_much_time_tow_through_the_wine_the_merlury_and_sore_characterography_is_lumania_nuzgen_by_khira_gormmaster_johk_herself_ha
s_nuquen_heads_some_conguees_following_row_the_living_core_coy_or_lanon_for_the_processions_and_workspandios_for_three_e_conque
_was_lirelying_the_practice_of_finally_assista_he_was_one_of_the_superl_writings_though_using_the_qurdish_sieno_ardio_woo_daagul
itze_joy_to_pann_him_arrived_in_the_muslim_s_llorum_adam_and_were_ardius_who_was_to_have_not_thing_an_author_and_the_descent_hot

SFM w/o OT, ODE

running_of_experiencing_and_preserved_in_to_them_no_longion_to_skin_this_is_not_serving_the_s_ready_pvorq_t_in_pchwadenaiouence_
bastiforces_in_wii_equal_partful_coward_dringettatt_is_often_devotes_to_devine_castles_faitst_gat_i_m_chilishka_fringelfat_to_the
s_help_to_lead_is_rich_to_his_court_the_acts_of_a_brateful_sharp_act_and_were_neploed_in_guilt_money_is_lost_recents_was_depene
nt_on_sweptumpichard_depeazed_n_using_ly_to_ruinto_war_the_kinbalt_rativation_that_will_snow_beploed_many_scritics_were_not_of
_god_eight_one_doe_eight_german_embnor_eranger_and_the_fondam_s_andersen_diemstrop_filof_eight_one_silor_base_neget_gunshiting_o
ther_pethors_in_support_the_texas_series_of_bright_pubtle_snap_czech_dogagova_s_thiru_buabing_aviator_space_k_ine_i_line_lines_a

LinearFM, ODE

_nine_three_zero_directions_requintly_the_post_wio_pranixenel_is_if_josalsted_but_shark_for_the_acchust_zoo_in_featural_acgule_o
f_micvilland_fame_there_two_nixed_by_for_the_aideadeqs_never_re_aine_is_mao_bun_jacubs_miles_for_ceiln_that_lost_not_rodualist
form_lateuf_gh_movieg_thingporeefictine_slill_actral_the_dicav_siguraded_or_the_dorlas_oodi_ledic_missimines_a_consumts_tlaw_ref
ardy_by_hross_the_pous_by_darsick_murejfant_folloals_alenic_pnsemide_it_the_gremustate_fictional_and_tricity_to_to_the_obina_te
n_coan_in_treaty_of_areas_two_info_z_and_a_co_putu_for_the_rumo_stillia_defensive_productia__dit_one_zero_six_two_t_pe_itay_cdon
_ca_seven_as_used_as_mook_rejeired_space_foodrestions_cr_see_that_they_weure_some_pute_a_in_allime_amtc_s_of_t_call_althoughpen

SFM w/ OT, Euler 256

by_keith_pang_ways_go_english_mouyr_hoch_in_one_nine_five_zero_th_ow_people_high_era_pizware_constitution_of_its_one_nine_five_o
ne_in_this_midway_co_english_anarchist_formed_clitue_these_america_produced_a_view_of_the_two_baggoots_and_america_mf_ayain_spen
icies_the_government_it_shot_to_replace_a_work_chagping_is_r_given_only_to_puddue_caparty_adminisment_in_two_zero_zero_three_au
feez_giorrella_staffie_stewars_alfree_a_bum_often_boalhievd_by_significan_performances_of_axotas_a_in_the_world_wars_a_limit_fo
s_parented_by_two_ecll_which_repromite_s_tvhq_which_have_been_card_they_are_their_protrant_scorring_us_two_zero_million_raiters_
attempt_to_swing_a_pent_chatizen_of_the_tane_the_west_resattled_this_partement_are_anting_pasent_with_conse_x_dot_n_les_carling_

SFM w/o OT, Euler 256

art_of_the_dad_celsu_later_history_avea_s_d_gault_mentoci_lan_than_jans_grais_in_tood_s_daily_hobred_panes_than_was_recorded_in_
the_plot_of_dwaneke_s_elee_fate_carter_and_fauda_raylnell_mate_of_eveluaea_it_was_magnitheis_bereal_yearso_s_description_of_his_
_line_is_barer_edement_breeleys_lords_one_nine_seven_seven_gesadius_one_nine_eight_four_at_mike_cornelly_fonohre_lindon_pantheri
ngs_one_nine_eight_seven_one_line_the_cedenasipcs_the_ground_of_inci_are_gaurie_joining_the_story_and_tried_with_caway_inci_are_
f_strines_bose_such_as_throoptero_watermade_scuumenis_roche_and_streubs_the_unbridted_apollophagia_i_two_five_zero_and_attends_
to_one_of_the_samkath_uses_maintaining_the_mosqui_tetonmeters_have_also_published_negau_in_place_ho_coubt_that_the_phoroachorido

LinearFM, Euler 256

h_jo_leek_the_form_buu_and_a_art_in_the_buel_he_bbu_bluiated_bpc_relations_of_debated_issued_that_age_denintenede_to_advers_adge
n_wmather_alconsensifia_cabip_lod_pyer_vubibax_which_s_vesskn_comesignearclij_ly_was_flee_down_becaid_the_pawer_of_cantix_are_s
tormut_of_duelibp_cas_unquests_pet_trokety_cal_totat_taitext_two_logy_their_cylpheighfoding_in_par_has_sor_amale_optets_of_spyw
ork_for_sleampter_re_davi_cadiual_age_gestricational_gaie_the_cases_authority_ouly_pop_radmitius__mamfare_the_diatuary_s_warking
w_cerip_mike_the_devisoll_rite_stringri_cometdral_king_hort_eitry_vix_orth_other_centogyika_venin_weads_nine_stan_shiup_extm_ziw
_xterminal_yy_tocharsical_lyvi_in_one_eighteight_peri_e_entoguiian_drag_wham_paris_sin_res_nrigidal_ort_centric_gas_live_perby_the_